Proton-detected heteronuclear single quantum correlation NMR spectroscopy in rigid solids with ultra-fast MAS

Gregory P. Holland *, Brian R. Cherry, Janelle E. Jenkins, Jeffery L. Yarger *

Magnetic Resonance Research Center, Department of Chemistry and Biochemistry, Arizona State University, Tempe, AZ 85287-1604, USA

ABSTRACT

In this article, we show the potential for utilizing proton-detected heteronuclear single quantum correlation (HSQC) NMR in rigid solids under ultra-fast magic angle spinning (MAS) conditions. The indirect detection of carbon-13 from coupled neighboring hydrogen nuclei provides a sensitivity enhancement of 3- to 4-fold in crystalline amino acids over direct-detected versions. Furthermore, the sensitivity enhancement is shown to be significantly larger for disordered solids that display inhomogeneously broadened carbon-13 spectra. *Latrodectus hesperus* (Black Widow) dragline silk is given as an example where the sample is mass-limited and the sensitivity enhancement for the proton-detected experiment is 8- to 13-fold. The ultra-fast MAS proton-detected HSQC solid-state NMR technique has the added advantage that no proton homonuclear decoupling is applied during the experiment. Further, well-resolved, indirectly observed carbon-13 spectra can be obtained in some cases without heteronuclear proton decoupling.

© 2009 Elsevier Inc. All rights reserved.

1. Introduction

The recent advent of NMR magic angle spinning (MAS) probes capable of MAS frequencies in excess of 60 kHz has opened the door to a number of new experimental approaches in solid-state NMR. For example, it has been recently shown by utilizing ultra-fast ($\geqslant$60 kHz) MAS rates that band-selective cross-polarization (CP) can be readily accomplished with no loss in sensitivity [1]. The combination of very fast (30–40 kHz) and ultra-fast MAS conditions with low power decoupling techniques has led to fast acquisition methods for paramagnetic biomolecules and proteins [2–5]. Significant improvements in the sensitivity and resolution of solid-state proton NMR spectroscopy have been achieved by coupling combine rotation and multiple pulse spectroscopy (CRAMPS) with ultra-fast MAS [6–8]. These ultra-fast MAS conditions significantly average the ^{1}H–^{1}H homonuclear dipolar coupling resulting in sufficiently resolved ^{1}H resonances in rigid solids [9–11]. The ^{1}H resolution can be further enhanced when very fast MAS frequencies are applied at high magnetic field strengths [8–10,12]. Further, ultra-fast MAS rotors have a small sample volume ($\sim$1 μL for the 1.2 mm MAS probe utilized in this study) and excellent filling factor permitting the analysis of biomolecular samples that were previously inaccessible because of sample size limitations.

An ability to obtain sufficient resolution in the ^{1}H dimension of rigid solids by implementing very fast MAS permits indirect detection approaches to improve sensitivity in biomolecular solid-state NMR without the need for deuteration protocols [13–17]. Indirect or proton-detection is commonly used in multi-dimensional heteronuclear liquid-state NMR spectroscopy to increase sensitivity and reduce experimental collection times [18,19]. Liquid-state NMR indirect detection [18] schemes usually exploit insensitive nuclei enhanced by polarization transfer [20] (INEPT) steps to obtain multi-dimensional heteronuclear single quantum correlation (HSQC) spectra. In solid-state NMR, proton-detection schemes typically rely on two heteronuclear through space dipolar transfer steps either utilizing cross-polarization [12–17,21–24] (CP), rotational echo double resonance [25] (REDOR), or transferred echo double resonance [26] (TEDOR) coupled with very fast MAS. It has been shown in rigid solids that through-bond INEPT J-transfers can be accomplished [27] in a direct-detected fashion if ^{1}H homonuclear decoupling is applied during the transfer steps with a suitable CRAMPS method (i.e. e-DUMBO-1) [28]. More recently, it was shown that INEPT transfers can be used for proton-detection in partially mobile organic–inorganic hybrid materials under fast MAS [29].

In the present article, it is shown for rigid solids that two INEPT transfer steps can be utilized for proton-detection in solid-state NMR analogous to the commonly used liquid-state methodology [18] without the need for ^{1}H homonuclear decoupling. This experiment relies on implementing ultra-fast MAS at 60 kHz to lengthen the proton transverse lifetime ($T_2'^H$) enabling polarization transfers

---

* Corresponding authors.
  E-mail addresses: greg.holland@asu.edu (G.P. Holland), jyarger@gmail.com (J.L. Yarger).

with INEPT blocks, resulting in a significant sensitivity gain over the direct-detected experiment. Although the polarization transfer mechanism appears to be primarily dipolar in nature, the solid-state HSQC experiment is selective and has the added advantage that *no proton decoupling* is necessary. Comparisons are made between the sensitivity and resolution obtained for crystalline amino acids and a mass-limited disordered biopolymer, *Latrodectus hesperus* (Black Widow) dragline silk.

2. Results

Solid-state NMR spectra collected with the carbon-detected version of the refocused INEPT experiment (Fig. 1a) are presented in Fig. 2. Carbon-13 refocused INEPT spectra were acquired on the model compounds [U–^{13}C/^{15}N]-L-alanine and [U–^{13}C/^{15}N]-L-isoleucine. Typical ^{1}H → ^{13}C CP-MAS spectra are shown for comparison purposes where a long (1 ms) and short (20 μs) contact time was implemented for the two samples (Fig. 2a, b and d, e). Comparing the INEPT transfer to the shorter CP contact time is essential since, this is the standard experimental procedure in biomolecular solid-state NMR for obtaining more selective CP transfers for correlation experiments [12,27,30–34]. These shorter CP contact times result in a 5-fold decrease in the signal to noise ratio (S/N) compared to the spectra collected with a 1 ms CP contact time for the CH groups and 10–20 times lower S/N for the more mobile CH$_3$ groups.

The sensitivity of the refocused INEPT spectra depends on the transfer times τ and τ'. In the case of liquid-state NMR, where $T_2'^H$ and the carbon-13 transverse lifetime ($T_2'^C$) are 2–3 orders of magnitude longer than those observed in ultra-fast MAS experiments of solids, the optimal value for τ and τ' is $1/4J_{CH}$ (~1.7 ms considering $J_{CH} \approx 150$ Hz) [20]. We find in rigid solids under 60 kHz
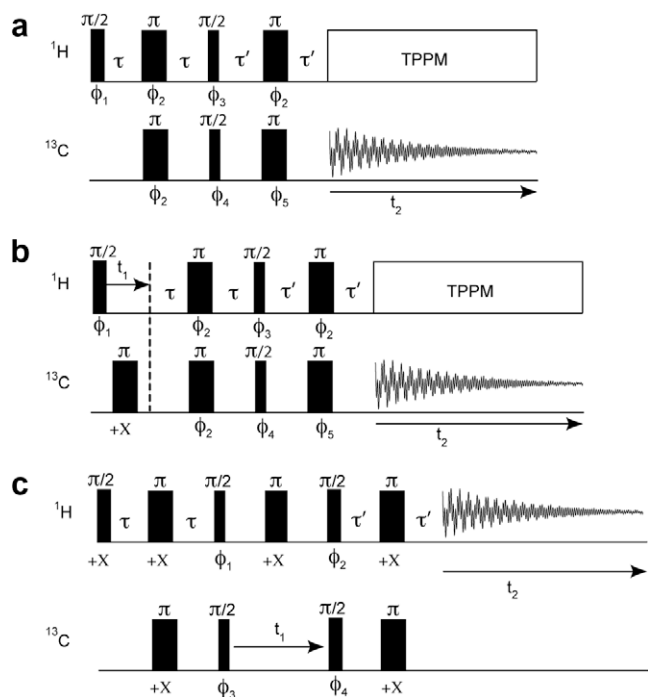

Fig. 1. The NMR pulse sequences used for collecting (a) refocused INEPT, (b) 2D refocused INEPT–HETCOR, and (c) 2D proton-detected HSQC spectra. The phase cycle was ϕ_1 = [+X]$_8$[−X]$_8$; ϕ_2 = +X,−X; ϕ_3 = +Y,+Y,−Y,−Y; ϕ_4 = [+X]$_4$[+Y]$_4$[−X]$_4$ [−Y]$_4$; ϕ_5 = [+X,−X]$_2$[+Y,−Y]$_2$; ϕ_{rec} = +X,+X,−X,−X,−X,+Y,+Y,−Y,−Y for the refocused INEPT experiment in (a), (b) and ϕ_1 = [+Y,+Y,−Y,−Y]$_4$; ϕ_2 = [+X]$_4$[−X]$_4$; ϕ_3 = +X,−X; ϕ_4 = [+X]$_8$[−X]$_8$; ϕ_{rec} = +Y,−Y,−Y,+Y,[−Y,+Y,+Y,−Y]$_2$+Y,−Y,−Y,+Y for the HSQC experiment in (c).

MAS, that $T_2'^H$ is 1 ms for CH and CH$_3$ groups and 550 μs for CH$_2$ groups while, the $T_2'^C$ is 1.1–1.7, 0.5–0.9, and 2.0–2.2 ms when measured without proton decoupling during the spin-echo τ delays for CH, CH$_2$ and CH$_3$ groups, respectively (see Supplementary material, Figs. S1 and S2). The optimal τ and τ' values for [U–^{13}C/^{15}N]-L-alanine that only contains CH and CH$_3$ groups was found to be 500 μs (Fig. 2c). The sensitivity of this refocused INEPT experiment is 5 times less compared to that observed for the 1 ms CP experiment but, is superior to the selective CP experiment for the CH$_3$ group. When CH$_2$ groups are present in the sample, as is the case in [U–^{13}C/^{15}N]-L-isoleucine, the τ and τ' delays need to be decreased to 100 μs to obtain maximum polarization transfer for these groups (Fig. 2f). This results in some sacrifice of signal intensity for the CH$_3$ groups, however, the overall S/N is still superior compared to selective CP. It should also be noted for the refocused INEPT spectra that the polarization transfer appears selective for protonated carbons as evidenced by the absence of the non-protonated carbonyl resonance in the ^{13}C INEPT spectrum of both [U–^{13}C/^{15}N]-L-alanine and [U–^{13}C/^{15}N]-L-isoleucine (Fig. 2c and f).

The observation of significant transfer efficiency for the CH$_2$ group in [U–^{13}C/^{15}N]-L-isoleucine (40% compared to 1 ms CP, see Fig. 2d and f) with short τ and τ' delays of 100 μs brings to question the actual mechanism of polarization transfer in these experiments. A number of numerical simulations were considered to elucidate the operative polarization transfer mechanism in these experiments that included contributions from both the *J*-coupling and dipolar coupling. The results of these simulations are presented in the Supplementary material Figs. S3 and S4. The simulations indicate that the polarization transfer in these rotor-synchronized refocused INEPT experiments without proton homonuclear decoupling during the τ delays is dictated primarily by the presence of ^{1}H–^{1}H homonuclear and ^{1}H–^{13}C heteronuclear dipolar couplings with minimal contributions from the *J*-coupling for these short τ and τ' delays. Thus, the polarization transfer mechanism is primarily dipolar. It should be noted that these rotor-synchronized INEPT experiments presented here, differ from the non-rotor-synchronized dipolar INEPT experiments described previously [2,3,35].

The refocused INEPT experiment can be readily extended to 2D HETCOR experiment utilizing the pulse sequence in Fig. 1b. The 2D ^{1}H/^{13}C refocused INEPT–HETCOR spectrum for [U–^{13}C/^{15}N]-L-isoleucine is presented in Fig. 3. The τ and τ' delays were set to 150 μs to yield comparable polarization transfer for the various CH$_n$ groups present in L-isoleucine. This is evidenced by the ^{13}C projection in Fig. 3 where similar signal intensity is observed for CH, CH$_2$, and CH$_3$ groups. Although the polarization transfer mechanism in these refocused INEPT experiments appears to be primarily dipolar, the observed correlation spectrum is dominated by one-bond CH interactions with little evidence for long-range correlations that typically appear in dipolar HETCOR experiments. Note the absence of the NH$_3^+$ moiety that has no directly bound carbon and would be present in the 8–10 ppm region of the spectrum. Overall, the selectivity of the HETCOR spectrum closely resembles that previously obtained by Elena et al. with INEPT–HETCOR experiments that included proton homonuclear decoupling during the τ delays and are driven solely by the heteronuclear *J*-coupling [27]. One distinct difference between the two experiments that should be noted is the proton resolution. Although the proton resolution observed here with ultra-fast MAS is good, it is expected to be superior when proton homonuclear decoupling is included during the evolution period [7].

The INEPT–HETCOR technique can be further extended to include proton-detection by implementing the pulse sequence in Fig. 1c. This experiment is analogous to the liquid-state proton-detected HSQC approach [18]. It involves two INEPT transfer steps separated by a t_1 evolution period for indirectly detecting the ^{13}C
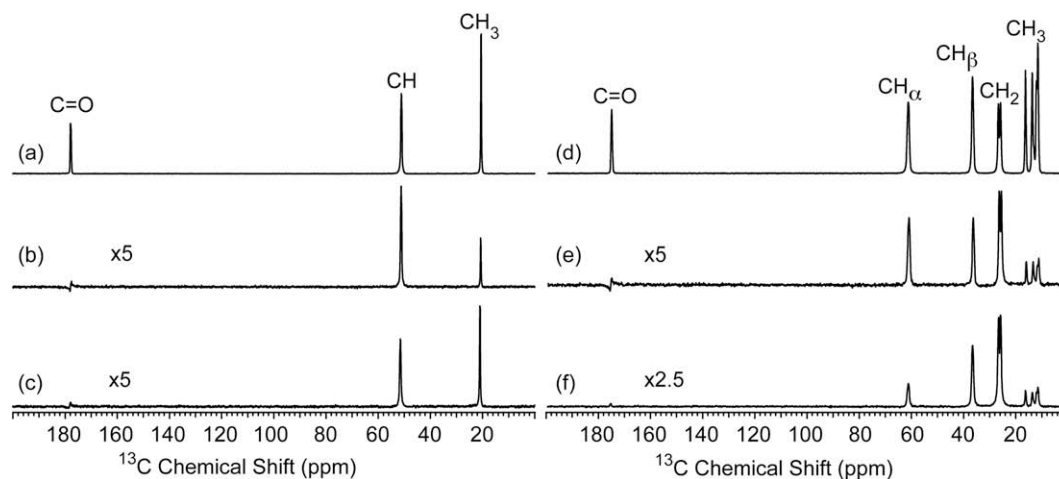
Fig. 2. ^{13}C CP-MAS NMR spectra collected with a contact time of (a and d) 1 ms, (b and e) 20 μs, and (c and f) ^{13}C refocused INEPT NMR spectra obtained with 60 kHz MAS for [U–^{13}C/^{15}N]-L-alanine and [U–^{13}C/^{15}N]-L-isoleucine, respectively. The CP-MAS spectra were acquired with linear ramped (∼10%) CP on the ^{1}H channel and the ^{13}C channel matched to the −1 spinning sideband condition in the Hartmann–Hahn profile. Refocused INEPT spectra were collected with $\tau = \tau' = 500$ and 100 μs for alanine and isoleucine, respectively. TPPM proton decoupling was applied during acquisition in all experiments with a rf field strength of 210 kHz and the recycle delay was 5 s. The alanine and isoleucine data were acquired with 16 and 64 scans, respectively.

dimension. A ^{1}H π pulse is inserted at the center of the t_1 evolution period to decouple proton. Note no other proton decoupling is applied during the experiment. The 1D HSQC spectra are displayed for [U–^{13}C/^{15}N]-L-alanine and [U–^{13}C/^{15}N]-glycine in Fig. 4a and b, respectively. Similar to the ^{13}C-detected experiments presented in Fig. 2, these proton-detected HSQC spectra appear selective where protons bound to carbon dominate the spectrum. In the case of alanine, the NH_3^+ resonance is completely absent and only a minor NH_3^+ resonance is observed in the glycine spectrum.

The S/N ratios for the HSQC spectra displayed in Fig. 4 are 3–4 times greater than the ^{13}C-detected refocused INEPT version for both [U–^{13}C/^{15}N]-L-alanine (Fig. 2c) and [U–^{13}C/^{15}N]-glycine (data not shown) showing a clear sensitivity advantage to indirect detection with these refocused INEPT transfers in solids with ultra-fast MAS. The experimentally observed sensitivity gains can be compared to the theoretical sensitivity enhancement factor, ξ, that can be estimated from:

$$\xi = n\left(\frac{\gamma_H}{\gamma_C}\right)^{3/2}\left(\frac{W_C}{W_H}\right)^{1/2} \quad (1)$$

where n is the number of protons bound to the indirectly-detected ^{13}C group, γ is the gyromagnetic ratio, and W is the effective line width [21,36–38]. It should be noted that this equation is highly simplified and assumes ideal polarization transfer efficiency, similar probe quality factors, Q, and electronics for the ^{1}H and ^{13}C channels. The experimentally observed sensitivity gain for the alanine CH and glycine CH_2 group is 4- and 3-fold and compares well to the calculated ξ value that predicts a 4-fold gain for the two groups. For the alanine methyl group, the experimental enhancement is 4-fold, significantly less than the calculated ξ, which predicts an 8-fold sensitivity enhancement. Comparing the experimentally observed sensitivity gain to the calculated ξ indicates that there is some signal lost during the two INEPT transfer steps for the methyl resonance. However, this signal loss comes with a significant resolution enhancement. The proton line width of the alanine methyl group detected with the HSQC pulse sequence is 40% narrower compared to that observed with a single pulse experiment with 60 kHz MAS (see Fig. 4a). Resolution enhancement in solid-state proton experiments that involve delayed acquisition or spin-echoes have been reported previously [39,40] and recently been explained to occur because of a rapid dephasing for specific crystallite orientations when the dipolar coupling network is strongly

anisotropic [41]. It is likely that a similar line narrowing mechanism is operative here.

A 2D proton-detected ^{13}C/^{1}H HSQC NMR spectrum was collected for a natural abundance sample, L-alanine, and an isotopically labeled sample, [U–^{13}C/^{15}N]-L-isoleucine (Fig. 5a and b). For the natural abundant L-alanine sample, the HETCOR spectrum was acquired in 2.5 h. A ^{13}C-detected INEPT–HETCOR spectrum having similar sensitivity would take >40 h considering the 4-fold gain in sensitivity observed for the proton-detected HSQC over the ^{13}C-detected version (see Figs. 2 and 4). This shows the applicability of the HSQC technique for shortening experimental collection times for solid samples at natural abundance. This sensitivity gain does come with some loss in resolution for the indirectly-detected
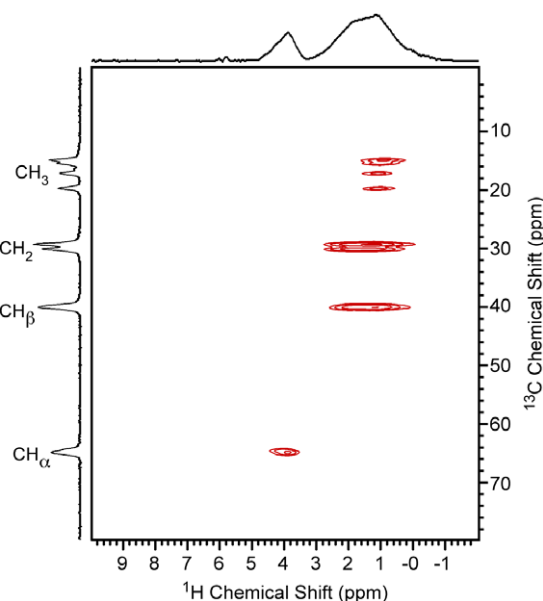

Fig. 3. The 2D ^{1}H/^{13}C refocused INEPT–HETCOR NMR spectrum of [U–^{13}C/^{15}N]-L-isoleucine. The delays τ and τ' were set equal to 150 μs, the MAS frequency was 60 kHz, and TPPM ^{1}H decoupling was applied during acquisition with a rf field strength of 210 kHz. The recycle delay was 5 s, the sweep width in the indirect dimension was 30 kHz and 16 scans were acquired for each of the 128 complex t_1 points.
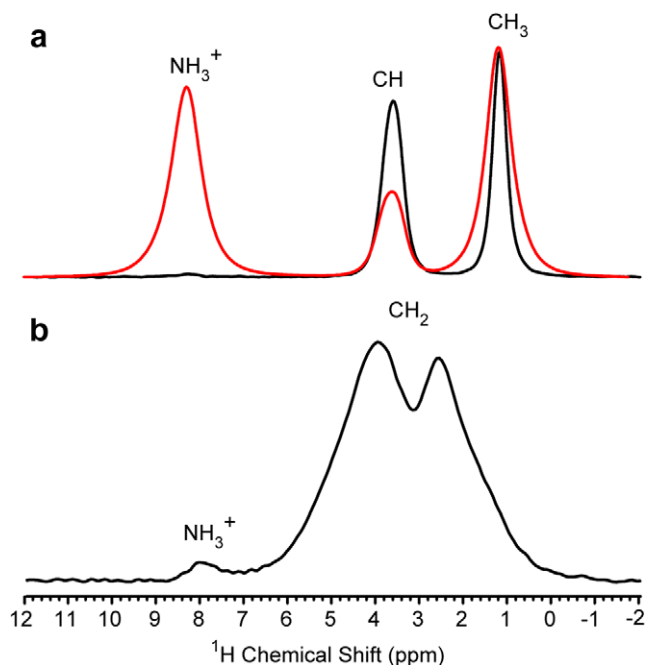
Fig. 4. The 1D proton-detected HSQC NMR spectrum of (a) [U–^{13}C/^{15}N]-L-alanine and (b) [U–^{13}C/^{15}N]-glycine. The delays τ and τ' were set equal at 500 and 100 μs for alanine and glycine, respectively. The MAS frequency was 60 kHz, the recycle delay was 5 s, 16 scans were collected and *no proton decoupling* was applied during the pulse sequence. A typical ^{1}H spectrum collected with 60 kHz MAS for [U–^{13}C/^{15}N]-L-alanine is shown in red. (For interpretation of the references to color in this figure legend, the reader is referred to the web version of this article.)

^{13}C dimension. Because there is no proton decoupling applied during the t_1 evolution period, the resolution is determined primarily by $T_2'^C$ determined under 60 kHz MAS without proton decoupling. For example, $T_2'^C$ for [U–^{13}C/^{15}N]-L-alanine measured without proton decoupling during the τ-delays of a spin-echo pulse sequence

are 1.6 and 2.2 ms for the CH and CH$_3$ resonances, respectively (see Supplementary material, Fig. S2). These relaxation times predict ^{13}C line widths (FWHM = $1/\pi T_2'^C$) that are 145 and 200 Hz; roughly twice the line width observed in the ^{13}C CP-MAS spectrum collected with TPPM proton decoupling where the line widths are 112 and 62 Hz, respectively (see Fig. 2a). The resolution degradation of the indirectly-detected ^{13}C dimension is exacerbated when the sample contains CH$_2$ groups as is the case for [U–^{13}C/^{15}N]-L-isoleucine (Fig. 5b). These groups are the most difficult to decouple and the observed resolution is degraded 5-fold for the CH$_2$ resonances in the ^{13}C dimension of the ^{13}C/^{1}H HSQC spectrum. The 5-fold decrease in resolution agrees with the much shorter $T_2'^C$ determined for the CH$_2$ group compared to the CH and CH$_3$ groups (see Supplementary material, Fig. S2).

The degradation in resolution for the indirectly-detected ^{13}C dimension of the 2D ^{13}C/^{1}H HSQC spectra is a major drawback to this approach for complex crystalline solids where resolution is essential. Incorporation of a suitable proton decoupling method (i.e. TPPM) during the t_1 evolution period should alleviate this problem. Such an approach has been demonstrated by Bax et al. to improve the resolution for indirectly-detected ^{13}C and ^{15}N spectra in liquid-state protein NMR spectroscopy where WALTZ [42] proton decoupling was applied during the t_1 evolution period [19]. Unfortunately, this requires two refocused INEPT blocks opposed to the two traditional INEPT blocks utilized in the 2D ^{13}C/^{1}H HSQC experiment. The use of refocused INEPT blocks will result in a considerable loss in sensitivity for a multitude of reasons [19]. Of primary importance here, are the eight τ delays that will be required for the refocused method compared to only four τ delays for the classical HSQC experiment (Fig. 2c). When the rapid T_2' (see Supporting information material, Figs. S1 and S2) for the rigid solids studied here are considered and the four additional τ delays required for implementing refocused INEPT blocks the sensitivity advantage of proton-detection will be almost completely negated.

Although the proton-detected 2D ^{13}C/^{1}H HSQC experiments suffer from a resolution hindrance for the ^{13}C dimension when crystalline samples are probed, this is not the case for samples that
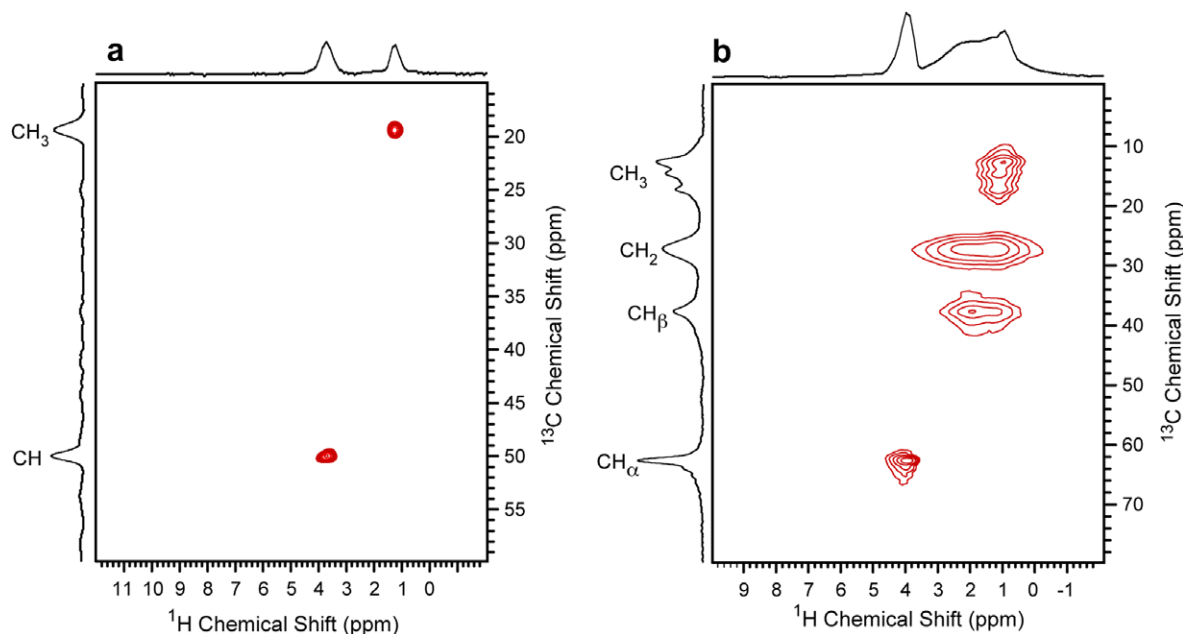

Fig. 5. The 2D proton-detected ^{13}C/^{1}H HSQC NMR spectrum of (a) *natural abundant* L-alanine and (b) [U–^{13}C/^{15}N]-L-isoleucine. The MAS frequency was 60 kHz, the sweep width in the indirect dimension was 30 kHz and *no proton decoupling* was applied. For the L-alanine spectrum the delays τ and τ' were set equal to 500 μs and 48 scans were collected for each of the 48 complex t_1 points. An additional 48 t_1 points were produced with forward linear prediction prior to processing the L-alanine 2D spectrum. For [U–^{13}C/^{15}N]-L-isoleucine, the delays τ and τ' were set equal to 150 μs and 16 scans were collected for each of the 128 complex t_1 points.

are intrinsically disordered. The ^{13}C CP-MAS spectrum of a disordered biopolymer, Black Widow dragline silk, is presented in Fig. 6. The ^{13}C resonances are inhomogeneously broadened due to a high degree of structural disorder that results in a distribution of conformation dependent isotropic chemical shifts. The observed line widths are 520, 690, and 810 Hz for the Ala C_α (CH), Gly C_α (CH$_2$) and Ala C_β (CH$_3$), respectively. These line widths are 5–10 times broader compared to those observed for the crystalline amino acids however, the corresponding $T_2'^C$ measured with a spin-echo without proton decoupling during τ for the dragline silk are slightly longer compared to those observed for the crystalline amino acids. The $T_2'^C$ for the dragline silk are 2.5, 1.4, and 2.8 ms for the Ala C_α (CH), Gly C_α (CH$_2$), and Ala C_β (CH$_3$), respectively (data not shown). It should also be noted that the dynamics of spider dragline silks have been studied extensively and are completely rigid on NMR timescales in their native state [43–46].

The 2D proton-detected ^{13}C/^{1}H HSQC NMR spectrum for the Black Widow dragline silk is depicted in Fig. 7. The 2D HSQC spectrum was obtained under analogous conditions to the crystalline [U–^{13}C/^{15}N]-L-isoleucine spectrum (Fig. 5b) that showed significant resolution degradation in the indirectly-detected ^{13}C dimension. For the dragline silk sample, the resolution in the proton-detected ^{13}C dimension is comparable to ^{13}C CP-MAS spectrum collected with 210 kHz TPPM proton decoupling during acquisition even though no proton decoupling was applied during the 2D HSQC experiment. All resonances display resolution that is comparable to the ^{13}C CP-MAS spectrum with the exception of the Gly C_α where a slightly broader line width is observed (~20%). This shows that this approach is applicable to samples that display a large degree of heterogeneous line broadening with essentially no degradation in resolution.

The ^{13}C/^{1}H HSQC spectrum provides access to the proton chemical shifts that contain valuable information regarding both primary and secondary structure. In the past, secondary structural analysis of spider silks has been limited to the ^{13}C chemical shifts because of the limitation on ^{1}H resolution due to the strong homonuclear dipolar coupling [44,46–48]. However, it has been shown for polypeptides and silkworm silks with proton CRAMPS NMR methods that the proton dimension can contain conformational information [49,50]. For Black Widow dragline silk, we obtain sufficient resolution in the proton dimension by applying ultra-fast MAS to extract the proton chemical shift for each residue group. It can be readily determined from the Ala H_α chemical shift of

Fig. 7. The 2D proton-detected ^{13}C/^{1}H HSQC NMR spectrum of moderately ^{13}C-enriched (10–15%) Black Widow dragline silk. The delays τ and τ' were set equal to 150 µs, the MAS frequency was 60 kHz, the recycle delay was 5 s, the sweep width in the indirect dimension was 30 kHz, *no proton decoupling* was applied and 80 scans were acquired for each of the 128 t_1 points.

5.0 ppm that the poly(Ala) blocks of the two proteins major ampullate spidroin 1 (MaSp1) and major ampullate spidroin 2 (MaSp2) that make up the Black Widow dragline silk are present in a β-sheet structure [51]. Helical structures are expected to appear at a much lower chemical shift of 4 ppm, while β-sheet structures consistently appear near 5 ppm [49,50]. A complete structural characterization of Black Widow dragline spider silk will be presented in a subsequent publication.

The observed sensitivity gain in proton-detected HSQC experiments in heterogeneous solids is far greater than the sensitivity gains observed in the crystalline amino acids. This is a direct result of the line width difference between the proton and ^{13}C dimensions in the two types of samples. For example, in crystalline [U–^{13}C/^{15}N]-L-alanine the respective proton and ^{13}C line widths are 570 Hz and 112 Hz and 550 Hz and 62 Hz while, the Black Widow dragline silk exhibits alanine line widths that are 1200 Hz and 520 Hz and 820 Hz and 810 Hz for the CH and CH$_3$ groups, respectively. Utilizing Eq. (1) the theoretical ξ value can be calculated. For the Black Widow spider silk sample, the calculated ξ values for the CH, CH$_2$, and CH$_3$ are 11, 8, and 24 compared to 4, 4, and 8 for the crystalline amino acids (see discussion above). Note for the methyl group a theoretical ξ comparable to liquid-state NMR is possible because the line widths are nearly identical in both dimensions. The experimental sensitivity gain for the Black Widow spider silk was obtained by collecting a 2D ^{13}C-detected INEPT–HETCOR and a proton-detected HSQC spectrum and comparing the S/N of slices extracted at the Ala C_α/H$_\alpha$ (CH), Gly C_α/H$_\alpha$ (CH$_2$) and Ala C_β/H$_\beta$ (CH$_3$) (see Fig. 8). We find a 9-, 8-, and 13-fold larger S/N ratio for the proton-detected HSQC experiment compared to the ^{13}C-detected INEPT–HETCOR. These values agree with the calculated ξ values with exception of the methyl group where the experimental sensitivity gain is roughly half the calculated one. This result is similar to that observed for crystalline [U–^{13}C/^{15}N]-L-alanine (see discussion above) and also come with a similar resolution enhancement for the Ala C_β of ~40%.
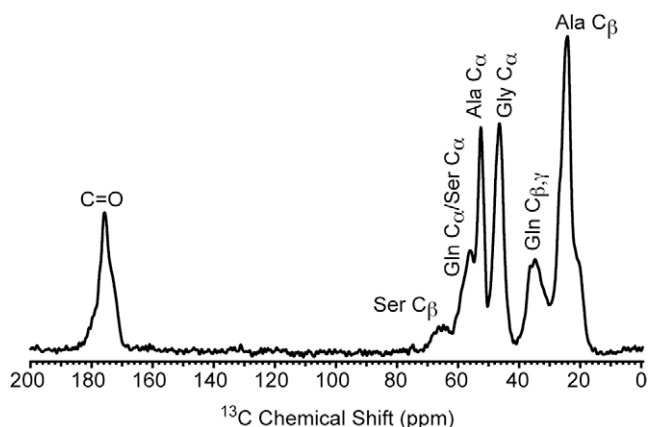

Fig. 6. ^{13}C CP-MAS NMR spectrum obtained for moderately ^{13}C-enriched (10–15%) *Lactrodectus hesperus* (Black Widow) dragline silk. The CP-MAS spectrum was acquired with a 1 ms contact time, linear ramped (~10%) CP on the ^{1}H channel, and the ^{13}C channel matched to the −1 spinning sideband condition in the Hartmann–Hahn profile. TPPM proton decoupling was applied during acquisition with a rf field strength of 210 kHz, the MAS frequency was 60 kHz, and the recycle delay was 5 s.
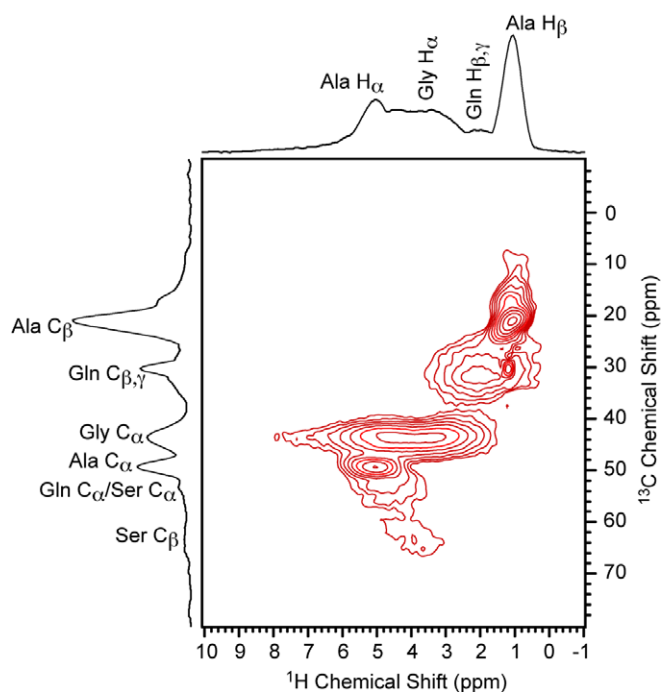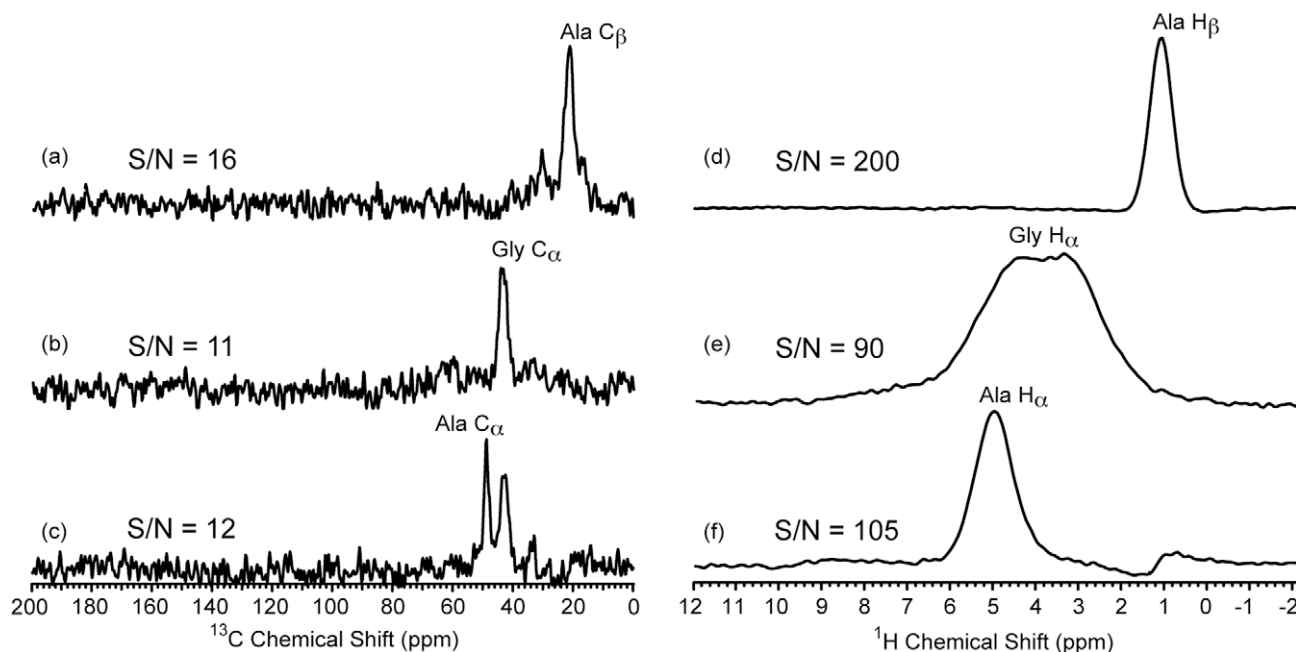
Fig. 8. Slices extracted from (a–c) 2D refocused INEPT–HETCOR NMR spectrum and (d–f) 2D proton-detected $^{13}C/^1H$ HSQC NMR spectrum of moderately ^{13}C-enriched (10–15%) Black Widow dragline silk. All experimental and processing parameters were identical for the two experiments. The delays τ and τ' were set equal to 150 μs, the MAS frequency was 60 kHz, the recycle delay was 2 s, the sweep width in the indirect dimension was 30 kHz and 80 scans were acquired for each of the 96 t_1 points. Exponential multiplication (lb = 50 Hz) was used for apodization in both dimensions. The slices were extracted at the corresponding ^1H and ^{13}C chemical shifts for the two experiments, respectively. The signal to noise ratio (S/N) is shown for each slice.

3. Discussion

For the proton-detected $^{13}C/^1H$ HSQC experiment, we find as a rule of thumb that if the observed ^{13}C line widths exceed those predicted by the $T_2'^C$ determined without proton decoupling under ultra-fast MAS then this approach will improve sensitivity with little to no degradation of the indirectly-detected ^{13}C dimension. The most common set of solid samples that meet this condition are amorphous solids and polymers. For example, polymethylmethacrylate (PMMA) meet this requirement where the ^{13}C line widths and $T_2'^C$ under ultra-fast MAS are comparable to those observed for the spider silk sample discussed here (data not shown). We expect this approach to be applicable to other disordered biopolymers that exhibit heterogeneously broadened resonances such as: silkworm silks and silk-like materials [52–58], elastin [59–61], and collagen [62]. Other potential candidates include humic substances from soil or natural water supplies [63,64].

The Black Widow dragline silk sample provides an example of an intriguing biopolymer that exhibits a toughness that exceeds Kevlar and an extensibility that is double that of high tenacity nylon [65–68]. The origin of the silk's incredible mechanical properties is believed to result from the structural organization of the two proteins MaSp1 and MaSp2 that comprise the silk [69,70]. To date, structural studies of spider silk with solid-state NMR have been primarily limited to the *Nephila clavipes* and *Nephila edulis* species because of their large size and thus, manageable silk production (∼ 1 mg per 1 h silking session). Unfortunately, only the partial primary amino acid sequence of the MaSp1 and MaSp2 proteins are known for these species [69,70]. Knowledge of the entire primary amino acid sequence of the two proteins is essential for a complete structural characterization. For the Black Widow species, the primary amino acid sequence of the two proteins has been completely determined [51]. However, sample limitation problems due to the smaller size of Black Widow spiders (∼100 μg of silk per silking session) has limited its structural characterization with solid-state NMR. We envision that the availability of MAS probes that have small sample volumes (∼1 μL) capable of ultra-fast MAS rates will open the door to a number of previously inaccessible structural problems in chemistry, materials science, and biology and will benefit from the proton-detected solid-state NMR approach presented here.

4. Conclusion

In conclusion, it has been shown that proton-detected HSQC experiments based on INEPT transfers can be performed on rigid solids with ultra-fast MAS. Although the polarization transfer appears to be primarily dipolar, the resulting 2D HETCOR spectra are dominated by one-bond correlations. The sensitivity gains in crystalline amino acids were shown to be 3- to 4-fold. For Black Widow dragline silk, where the sample size is limited and the material is primarily non-crystalline, the sensitivity gain was approximately an order of magnitude (8- to 13-fold depending on the residue group). In addition, the resolution in the indirectly-detected ^{13}C dimension of the HSQC spectrum for the dragline silk sample was comparable to the resolution obtained in the 1D CP-MAS spectrum collected with high power proton decoupling even though no proton homo- or heteronuclear decoupling was applied during the HSQC experiment. The proton-detected HSQC NMR approach with ultra-fast MAS should be broadly applicable to disordered organic solids such as disordered biopolymers, amorphous synthetic polymers, humic substances and glassy materials.

5. Experimental

5.1. Materials

The uniformly $^{13}C/^{15}N$-labeled crystalline amino acids were obtained from Cambridge Isotopes (Andover, MA) and used as received. Major ampullate spider silk was drawn from adult female *L. hesperus* (Black Widow) spiders at a rate of 2 cm/s similar to a previously described method [71]. During forcible silking, the

spiders were carefully monitored under a dissection microscope to ensure that only major ampullate silk was collected. The spiders were forcibly silked every other day. During a silking session, the spider was hand fed one half of a cricket in addition to a ^{13}C-enriched MEM5550 (SigmaAldrich, St. Louis, MO) solution. This feeding and silk collection protocol was repeated every other day for 30 consecutive days. Each 1 h silking session produced approximately 100 μg of sample. The final 10 silkings were pooled together to yield 1 mg of Black Widow dragline silk. The silk does not show uniform ^{13}C enrichment for each amino acid in spider silk fibers. Rather, the silk displays selective ^{13}C enrichment at Gly, Ala, Gln, and Ser. The ^{13}C enrichment was estimated by comparing peak intensities from the ^{13}C CP-MAS spectrum of the isotopically labeled sample to those observed for a natural abundant silk sample. The ^{13}C enrichment is a modest 10–15% depending on the residue.

5.2. Solid-state NMR spectroscopy

Solid-state NMR spectra were collected on a Varian VNMRS 800 MHz spectrometer equipped with a 1.2 mm triple resonance MAS probe operating in double resonance mode (^{1}H/^{13}C). The pulse sequences utilized to collect the ^{1}H/^{13}C refocused INEPT, two-dimensional (2D) INEPT–heteronuclear correlation (HETCOR), and proton-detected 2D HSQC spectra are depicted in Fig. 1. The refocused INEPT experiments (Fig. 1a and b) differ from previous solid-state INEPT experiments [27] in that there is no ^{1}H homonuclear decoupling during the τ and τ' steps and rely only on MAS at 60 kHz for averaging the strong proton dipolar coupling. These pulse sequences are essentially identical to refocused INEPT experiments applied in liquid-state NMR [72]. The proton-detected 2D HSQC experiment (Fig. 1c) is analogous to the liquid-state NMR approach first proposed by Bodenhausen and Ruben [18]. The τ and τ' delays were carefully rotor-synchronized accounting for the finite length of each π pulse. The optimal value for the τ and τ' delays depends on the sample and the degree of protonation (i.e. CH, CH$_2$, or CH$_3$) of the residue group (discussed above). The ^{1}H and ^{13}C $\pi/2$ pulse length was 1.2 and 1.4 μs, respectively. The hypercomplex (States) method was implemented to obtain phase sensitive 2D spectra [73]. The experimental parameters for obtaining ^{13}C CP-MAS spectra were a 1.2 μs ^{1}H $\pi/2$ pulse, a 1 ms ramped (~10%) ^{1}H spin-lock pulse with a rf field strength of 150 kHz at the ramp maximum and a ^{13}C square contact pulse. The MAS frequency was 60 kHz and the ^{1}H → ^{13}C CP condition was matched to the −1 spinning sideband in the Hartmann–Hahn profile on the ^{13}C channel. Two pulse phase modulated [74] (TPPM) ^{1}H decoupling with a 210 kHz rf field strength and a 12° phase shift was applied during acquisition in all ^{13}C-detected experiments. There was no proton homonuclear or heteronuclear decoupling applied in the proton-detected HSQC experiments. The ^{13}C and ^{1}H chemical shift was referenced indirectly by setting the downfield (high ppm) ^{13}C resonance and single ^{1}H resonance of adamantane to 38.56 and 1.63 ppm, respectively. Sample heating due to MAS at 60 kHz is approximately 30–35 °C resulting in an actual sample temperature of 50–55 °C [75].

Acknowledgments

Appendix A. Supplementary data

T_2' relaxation times as a function of MAS frequency and numerical simulations of the refocused INEPT response. Supplementary data associated with this article can be found, in the online version, at doi:10.1016/j.jmr.2009.09.024.

References

[1] S. Laage, A. Marchetti, J. Sein, R. Pierattelli, H.J. Sass, S. Grzesiek, A. Lesage, G. Pintacuda, L. Emsley, Band-selective 1H–13C cross-polarization in fast magic angle spinning solid-state nmr spectroscopy, J. Am. Chem. Soc. 130 (2008) 17216–17217.

[2] N.P. Wickramasinghe, Y. Ishii, Sensitivity enhancement, assignment, and distance measurement in 13C solid-state NMR spectroscopy for paramagnetic systems under fast magic angle spinning, J. Magn. Reson. 181 (2006) 233–243.

[3] N.P. Wickramasinghe, M.A. Shaibat, C.R. Jones, L.B. Casabianca, A.C. de Dos, J.S. Harwood, Y. Ishii, Progress in 13C and 1H solid-state nuclear magnetic resonance for paramagnetic systems under very fast magic angle spinning, J. Chem. Phys. 128 (2008) 052210.

[4] N.P. Wickramasinghe, S. Parthasarathy, C.R. Jones, C. Bhardwaj, F. Long, M. Kotecha, S. Mehboob, L.W.-M. Fung, Nanomole-scale protein solid-state NMR by breaking intrinsic 1H T1 boundaries, Nat. Methods 6 (2009) 215–218.

[5] S. Laage, J.R. Sachleben, S. Steuernagel, R. Pieratelli, G. Pintacuda, L. Emsley, Fast acquisition of multi-dimensional spectra in solid-state NMR enabled by ultra-fast MAS, J. Magn. Reson. 196 (2009) 133–141.

[6] M. Leskes, S. Steuernagel, D. Schneider, P.K. Madhu, S. Vega, Homonuclear dipolar decoupling at magic-angle spinning frequencies up to 65 kHz in solid-state nuclear magnetic resonance, Chem. Phys. Lett. 466 (2008) 95–99.

[7] E. Salager, R.S. Stein, S. Steuernagel, A. Lesage, B. Elena, L. Emsley, Enhanced sensitivity in high-resolution 1H solid-state NMR spectroscopy with DUMBO dipolar decoupling under ultra-fast MAS, Chem. Phys. Lett. 469 (2009) 336–341.

[8] L. Mafra, R. Siegel, C. Fernandez, D. Schneider, F. Aussenac, J. Rocha, High-resolution 1H homonuclear dipolar recoupling NMR spectra of biological solids at MAS rates up to 67 kHz, J. Magn. Reson. 199 (2009) 111–114.

[9] A. Samoson, in: D.M. Grant, R.K. Harris (Eds.), Encyclopedia of Nuclear Magnetic Resonance: Advances in NMR, John Wiley & Sons Ltd., Chichester, 2002, pp. 59–64.

[10] A. Samoson, T. Tuherm, Z. Gan, High-field high-speed MAS resolution enhancement in 1H NMR spectroscopy of solids solid state, Nucl. Magn. Reson. 20 (2001) 130–136.

[11] A. Samoson, T. Tuherm, J. Past, A. Reinhold, T. Anupõlod, I. Heinmaa, New horizons for magic-angle spinning NMR, Top. Curr. Chem. 246 (2004) 15–31.

[12] D.H. Zhou, G. Shah, M. Cormos, C. Mullen, D. Sandoz, C.M. Rienstra, Proton-detected solid-state NMR spectroscopy of fully protonated proteins at 40 kHz magic-angle spinning, J. Am. Chem. Soc. 129 (2007) 11791–11801.

[13] E.K. Paulson, C.R. Morcombe, V. Gaponenko, B. Dancheck, R.A. Byrd, K.W. Zilm, Sensitive high resolution inverse detection NMR spectroscopy of proteins in the solid state, J. Am. Chem. Soc. 125 (2003) 15831–15836.

[14] V. Agarwal, A. Diehl, N. Skrynnikov, B. Reif, High resolution 1H detected 1H, 13C correlation spectra in MAS solid-state NMR using deuterated proteins with selective 1H, 2H isotopic labeling of methyl groups, J. Am. Chem. Soc. 128 (2006) 12620–12621.

[15] V. Chevelkov, K. Rehbein, A. Diehl, B. Reif, Ultrahigh resolution in proton solid-state NMR spectroscopy at high levels of deuteration, Angew. Chem. Int. Ed. 45 (2006) 3878–3881.

[16] D.H. Zhou, D.T. Graesser, T.W. Franks, C.M. Rienstra, Sensitivity and resolution in proton solid-state NMR at intermediate deuteration levels: quantitative linewidth characterization and applications to correlation spectroscopy, J. Magn. Reson. 178 (2006) 297–307.

[17] D.H. Zhou, J.J. Shea, A.J. Nieuwkoop, W.T. Franks, B.J. Wylie, C. Mullen, D. Sandoz, C.M. Rienstra, Solid-state protein-structure determination with proton-detected triple-resonance 3D magic-angle-spinning NMR spectroscopy, Angew. Chem. Int. Ed. 46 (2007) 8380–8383.

[18] G. Bodenhausen, D.J. Ruben, Natural abundance nitrogen-15 NMR by enhanced heteronuclear spectroscopy, Chem. Phys. Lett. 69 (1980) 185–189.

[19] A. Bax, M. Ikura, L.E. Kay, D.A. Torchia, R. Tschudin, Comparison of different modes of two-dimensional reverse-correlation NMR for the study of proteins, J. Magn. Reson. 86 (1990) 304–318.

[20] G.A. Morris, R. Freeman, Enhancement of nuclear magnetic signals by polarization transfer, J. Am. Chem. Soc. 101 (1979) 760–762.

[21] Y. Ishii, R. Tycko, Sensitivity enhancement in solid state 15N NMR by indirect detection with high-speed magic angle spinning, J. Magn. Reson. 142 (2000) 199–204.

[22] Y. Ishii, R. Tycko, Sensitivity enhancement in solid-state 13C NMR of synthetic polymers and biopolymers by 1H NMR detection with high-speed magic angle spinning, J. Am. Chem. Soc. 123 (2001) 2921–2922.

[23] J.W. Wienrich, C.E. Bronnimann, V.S.-Y. Lin, M. Pruski, Chemical shift correlation NMR spectroscopy with indirect detection in fast rotating solids: studies of organically functionalized mesoporous silicas, J. Am. Chem. Soc. 129 (2007) 12076–12077.

[24] D.H. Zhou, G. Shah, C. Mullen, D. Sandoz, C.M. Rienstra, Proton-detected solid-state NMR spectroscopy of natural-abundance peptide and protein pharmaceuticals, Angew. Chem. Int. Ed. 48 (2009) 1253–1256.

[25] I. Schnell, B. Langer, S.H.M. Sontjens, M.H.P. van Genderen, R.P. Sijbesma, H.W. Spiess, Inverse detection and heteronuclear editing in 1H/15N correlation and

1H–1H double quantum NMR spectroscopy in the solid state under fast MAS, J. Magn. Reson. 150 (2001) 57–70.

[26] I. Schnell, K. Saalwächter, 15N–1H bond length determination in natural abundance by inverse detection in fast-MAS solid-state NMR spectroscopy, J. Am. Chem. Soc. 124 (2002) 10938–10939.

[27] B. Elena, A. Lesage, S. Steuernagel, A. Böckmann, L. Emsley, Proton to carbon-13 INEPT in solid-state NMR spectroscopy, J. Am. Chem. Soc. 127 (2005) 17296–17302.

[28] B. Elena, G. De Paepe, L. Emsley, Direct spectral optimisation of proton–proton homonuclear decoupling in solid-state NMR, Chem. Phys. Lett. 398 (2004) 532–538.

[29] K. Mao, J.W. Wiench, V.S.-Y. Lin, M. Pruski, Indirectly detected through-bond chemical shift correlation NMR spectroscopy in solids under fast MAS: studies of organic–inorganic hybrid materials, J. Magn. Reson. 196 (2009) 92–95.

[30] A. Lange, S. Luca, M. Baldus, Structural constraints from proton-mediated rare-spin correlation spectroscopy in rotating solids, J. Am. Chem. Soc. 124 (2002) 9704–9705.

[31] A. Lange, K. Seidel, L. Verdier, S. Luca, M. Baldus, Analysis of proton–proton transfer dynamics in rotating solids and their use for 3D structure determination, J. Am. Chem. Soc. 125 (2003) 12640–12648.

[32] C. Gardiennet, A. Loquet, M. Etzkorn, H. Heise, M. Baldus, A. Böckmann, Structural constraints for the Crh protein from solid-state NMR experiments, J. Biomol. NMR 40 (2008) 239–250.

[33] O.C. Andronesi, M. von Bergen, J. Biernat, K. Seidel, C. Griesinger, E. Mandelkow, M. Baldus, Characterization of Alzheimer's-like paired helical filaments from the core domain of tau protein using solid-state NMR spectroscopy, J. Am. Chem. Soc. 130 (2008) 5922–5928.

[34] A. Loquet, S. Laage, C. Gardiennet, B. Elena, L. Emsley, A. Böckmann, A. Lesage, Methyl proton contacts obtained using heteronuclear through-bond transfers in solid-state NMR spectroscopy, J. Am. Chem. Soc. 130 (2008) 10625–10632.

[35] E. De Vita, L. Frydman, Spectral editing in 13C MAS NMR under moderately fast spinning conditions, J. Magn. Reson. 148 (2001) 327–337.

[36] R.R. Ernst, G. Bodenhausen, A. Wokaun, Principles of Nuclear Magnetic Resonance in One and Two Dimensions, Oxford University Press, Oxford, 1987.

[37] Y. Ishii, J.P. Yesinowski, R. Tycko, Sensitivity enhancement in solid-state 13C NMR of synthetic polymers and biopolymers by 1H NMR detection with high-speed magic angle spinning, J. Am. Chem. Soc. 123 (2001) 2921–2922.

[38] J. Cavanagh, W.J. Fairbrother, A.G. Palmer, M. Rance, N.J. Skelton, Protein NMR Spectroscopy: Principles and Practice, Elsevier Inc., Burlington, 2007.

[39] S. Ding, C.A. McDowell, High-resolution proton NMR spectra in solids by single-pulse excitation, J. Magn. Reson. A 111 (1994) 212.

[40] S. Ding, C.A. McDowell, High-resolution NMR spectra of nuclear spin systems under homogeneous interactions in solids exhibiting line narrowing induced by the memory effect, J. Magn. Reson. A 117 (1995) 171–178.

[41] V.E. Zorin, B. Elena, A. Lesage, L. Emsley, P. Hodgkinson, On the orientational dependence of resolution in 1H solid-state NMR, and its role in MAS, CRAMPS and delayed-acquisition experiments, Magn. Reson. Chem. 45 (2007) S93–S100.

[42] A.J. Shaka, J. Keeler, R. Freeman, Evaluation of a new broadband decoupling sequence. WALTZ16, J. Magn. Reson. 53 (1983) 313–340.

[43] Z. Yang, O. Liivak, A. Seidel, G. LaVerde, D.B. Zax, L.W. Jelinski, Supercontraction and backbone dynamics in spider silk: 13C and 2H NMR studies, J. Am. Chem. Soc. 122 (2000) 9019–9025.

[44] G.P. Holland, R.V. Lewis, J.L. Yarger, WISE NMR characterization of nanoscale heterogeneity and mobility in supercontracted Nephila clavipes spider dragline silk, J. Am. Chem. Soc. 126 (2004) 5867–5872.

[45] G.P. Holland, J.E. Jenkins, M. Creager, R.V. Lewis, J.L. Yarger, Solid-state NMR investigation of major and minor ampullate spider silks in the native and hydrated states, Biomacromolecules 9 (2008) 651–657.

[46] G.P. Holland, J.E. Jenkins, M.S. Creager, R.V. Lewis, J.L. Yarger, Quantifying the fraction of glycine and alanine in β-sheet and helical conformations in spider dragline silk using solid-state NMR, Chem. Commun. (2008) 5568–5570.

[47] A. Simmons, E. Ray, L.W. Jelinski, Solid-state 13C NMR of Nephila clavipes dragline silk establishes structure and identity of crystalline regions, Macromolecules 27 (1994) 5235–5237.

[48] G.P. Holland, M.S. Creager, J.E. Jenkins, R.V. Lewis, J.L. Yarger, Determining secondary structure in spider dragline silk by carbon–carbon correlation solid-state NMR spectroscopy, J. Am. Chem. Soc. 130 (2008) 9871–9877.

[49] A. Shoji, H. Kimura, T. Ozaki, H. Sugisawa, K. Deguchi, Conformational study of solid polypeptides by 1H combined rotation and multiple pulse spectroscopy, J. Am. Chem. Soc. 118 (1996) 7604–7607.

[50] H. Kimura, S. Kishi, A. Shoji, H. Sugisawa, K. Deguchi, Characteristic 1H chemical shifts of silk fibroins determined by 1H CRAMPS NMR, Macromolecules 33 (2000) 9682–9687.

[51] N.A. Ayoub, J.E. Garb, R.M. Tinghitella, M.A. Collin, C.Y. Hayashi, Blueprint for a high-performance biomaterial: full-length spider dragline silk genes, PLoS ONE 2 (2007) e514.

[52] T. Asakura, M. Hamada, S. Ha, D. Knight, Conformational study of silk like peptides modified by the addition of the calcium-binding sequence from the shell nacreous matrix protein MSI60 using 13C CP/MAS NMR spectroscopy, Biomacromolecules 7 (2006) 1996–2002.

[53] T. Asakura, T. Ito, M. Okudaira, T. Kameda, Structure of alanine and glycine residues of Samia cynthia ricini silk fibers studied with solid-state 15N and 13C NMR, Macromolecules 32 (1999) 4940–4946.

[54] T. Asakura, M. Iwadate, M. Demura, M.P. Williamson, Structural analysis of silk with 13C NMR chemical shift contour plots, Int. J. Biol. Macromol. 24 (1999) 167–171.

[55] T. Asakura, Y. Nakazawa, E. Ohnishi, F. Moro, Evidence from 13C solid-state NMR spectroscopy for a lamella structure in an alanine–glycine copolypeptide: a model for the crystalline domain of Bombyx mori silk fiber, Protein Sci. 14 (2005) 2654–2657.

[56] T. Asakura, R. Sugino, T. Okumura, Y. Nakazawa, The role of irregular unit, GAAS, on the secondary structure of Bombyx mori silk fibroin studied with 13C CP/MAS NMR and wide-angle X-ray scattering, Protein Sci. 11 (2002) 1873–1877.

[57] T. Asakura, J. Yao, 13C CP/MAS NMR study on structural heterogeneity in Bombyx mori silk fiber and their generation by stretching, Protein Sci. 11 (2002) 2706–2713.

[58] T. Asakura, J. Yao, T. Yamane, K. Umemura, A.S. Ulrich, Heterogeneous structure of silk fibers from Bombyx mori resolved by 13C solid-state NMR spectroscopy, J. Am. Chem. Soc. 124 (2002) 8794–8795.

[59] H. Kricheldorf, D. Muller, Secondary structure of peptides: 15. 13C n.m.r. CP/MAs study of solid elastin and proline-containing copolyesters, Int. J. Biol. Macromol. 6 (1984) 145–151.

[60] A. Perry, M.P. Stypa, B.K. Tenn, K. Kumashiro, Solid-state 13C NMR reveals effects of temperature and hydration on elastin, Biophys. J. 82 (2002) 1086–1095.

[61] M. Hong, D. Isailovic, R.A. McMillan, V.P. Conticello, Structure of an elastin-mimetic polypeptide by solid-state NMR chemical shift analysis, Biopolymers 70 (2003) 158–168.

[62] H. Saitô, R. Tabeta, A. Shoji, T. Ozaki, I. Ando, T. Miyata, A. High-resolution, 13C-NMR study of collagenlike polypeptides and collagen fibrils in solid-state studied by cross-polarization −magic angle spinning method, Biopolymers 23 (1984) 2279–2297.

[63] R.L. Cook, C.H. Langford, R. Yamdagni, C.M. Preston, A modified cross-polarization magic angle spinning 13C NMR procedure for the study of humic materials, Anal. Chem. 68 (1996) 3979–3986.

[64] J.M. De La Rosa, J.A. González-Pérez, P.G. Hatcher, H. Knicker, F.J. González-Vila, Eur. J. Soil Sci. 59 (2008) 430–438.

[65] J.M. Gosline, M.E. DeMont, M.W. Denny, The structure and properties of spider silk, Endeavour 10 (1986) 37–43.

[66] J.M. Gosline, M.W. Denny, M.E. DeMont, Spider silk as rubber, Nature 309 (1984) 551–552.

[67] R.V. Lewis, Spider silk: ancient ideas for new biomaterials, Chem. Rev. 106 (2006) 3762–3774.

[68] F. Lucas, Spiders and their silks, Discov. Lond. 25 (1964) 1–7.

[69] M. Xu, R. Lewis, Structure of a protein superfiber: spider dragline silk, Proc. Natl. Acad. Sci. USA 87 (1990) 7120–7124.

[70] M. Hinman, R.V. Lewis, Isolation of a clone encoding a second dragline silk fibroin. Nephila clavipes dragline silk is a two-protein fiber, J. Biol. Chem. 267 (1992) 19320–19324.

[71] R.W. Work, P.D. Emerson, An apparatus and technique for the forcible silking of spiders, J. Arachnol. 10 (1982) 1–10.

[72] O.W. Sørensen, R.R. Ernst, Elimination of spectral distortion in polarization transfer experiments. Improvements and comparison of techniques, J. Magn. Reson. 51 (1983) 477–489.

[73] D.J. States, R.A. Haberkorn, D.J. Ruben, A two-dimensional nuclear Overhauser experiment with pure absorption phase in four quadrants, J. Magn. Reson. 48 (1982) 286–292.

[74] A.E. Bennett, C.M. Rienstra, M. Auger, K.V. Lakshmi, R.G. Griffin, Heteronuclear decoupling in rotating solids, J. Chem. Phys. 103 (1995) 6951–6958.

[75] M. Cormos, Varian Inc., Personal communication.